Comparison of the Shielding Properties of Superconducting and Superconducting/Ferromagnetic Bi- and Multi-layer Systems

L. Gozzelino, R. Gerbaldo, G. Ghigo, F. Laviano, M. Truccato

Comparison of the shielding properties of superconducting and superconducting/ferromagnetic bi- and multi-layer systems

J Supercond Nov Magn **30**, 749–756 (2017)

DOI: 10.1007/s10948-016-3659-z

Comparison of the shielding properties of superconducting and superconducting/ferromagnetic bi- and multi-layer systems

L. Gozzelino[1,2], R. Gerbaldo[1,2], G. Ghigo[1,2], F. Laviano[1,2], M. Truccato[2,3]

(1) Department of Applied Science and Technology, Politecnico di Torino, C.so Duca degli Abruzzi 24, 10129 Torino, Italy
(2) Istituto Nazionale di Fisica Nucleare, Sezione di Torino, Via P. Giuria 1, 10125 Torino Italy
(3) Department of Physics and Nanostructured Interfaces and Surfaces Centre, Università di Torino, Via P. Giuria 1, 10125 Torino, Italy

Corresponding author:
Laura Gozzelino
e-mail: laura.gozzelino@polito.it
phone: +39-011-0907314
fax: +39-011-0907399

Abstract. This paper compares the shielding properties of superconducting (SC) and superimposed superconducting/ferromagnetic (SC/FM) systems, consisting of cylindrical cups with an aspect ratio of height/radius close to unity. Both bilayer structures, with the SC cup placed inside the FM one, and multilayer structures, made up of two SC and two FM alternating cups, have been considered. Induction magnetic field values have been calculated by means of a finite element model based on the vector potential formulation, simultaneously taking into account the non-linear properties of both the SC and the FM materials. The analysis highlights that at low applied fields the presence of a height difference between the edge of the SC/FM cups, as well as a suitable choice of the lateral gap between the cups, is a key factor in obtaining hybrid structures with a shielding potential comparable to, or even higher than, that of the single SC cup. In contrast, at high applied fields all the hybrid arrangements investigated always provide much greater shielding factors than the SC cup alone. The computation results show that at both low and high applied fields the multilayer solutions are the hybrid shields with the highest efficiency.

Keywords: magnetic shielding, superimposed superconducting/ferromagnetic systems, finite element model, MgB_2 bulk

1. Introduction

For their electromagnetic properties of perfect diamagnetism, superconducting (SC) materials are natural candidates for passive magnetic shields working in the low-frequency magnetic field range [1-3]. However, their use is restricted by the limited values of the maximum magnetic flux density they are able to shield. The superimposition of one or more ferromagnetic (FM) layers onto the SC shield has been proved, both by experiments [4-6] and by computing [7] to increase its efficiency in the magnetic field mitigation, even allowing the cloaking of dc and ac magnetic fields [8-10].

The best shielding results are expected to be achieved by inserting the ferromagnetic layer between the field source and the superconductor [7]. Furthermore, it has been demonstrated that the efficiency of this hybrid shield can be optimized either by means of a suitable shaping and sizing of the ferromagnet [7, 11-13] or by tuning the size of the gap between the walls of the SC and FM vessels [4, 13]. Investigations on tubular SC/FM shields, with an aspect ratio of height/radius higher than 10 and the FM layer positioned between the magnetic field source and the SC vessel, showed that in the centre of the screen the shielding factor (SF)[1] of the whole arrangement agreed, with a good approximation, with the product of the shielding factor of the single tubes [4, 7]. In contrast, this was not verified in superimposed SC/FM arrangements with a reduced aspect ratio of height/radius [6], where the shielding factor of the whole structure must be evaluated by means of dedicated experiments or modelling.

Several numerical techniques have been proposed for modelling superconductors [14, 15], even in presence of other materials with non-linear magnetic properties, such as ferromagnets [7, 9, 16, 17]. Among these, the finite element method techniques are the most commonly applied to the material study, using different formulations, such as the **H** (magnetic field) formulation [18], the **T**-Ω (current vector potential and magnetic potential) formulation [19] and the **A**-V (magnetic vector potential and electrostatic potential) formulation [20]. In the framework of this last formulation and starting from the approach proposed by Campbell [20, 21], Gömöry *et al.* [22] developed a critical state algorithm, which was successfully applied in the calculations of the magnetic flux penetration into SC/FM composites with non-linear properties of both the SC and the FM layers.

In previous papers we focused on the analysis of the magnetic shielding properties of MgB_2 and Fe cylindrical cups measured separately and in the superimposed configuration with the MgB_2 cup coaxially inserted in the Fe one [6, 12]. The external magnetic field, $\mu_0 H_{appl}$, was applied parallel to the cup axis. Both the MgB_2 and Fe cups were chosen with an aspect ratio of height/radius close to unity, in order to investigate magnetic mitigation solutions in a situation where it is necessary to

[1] The shielding factor produced by a magnetic shield is evaluated as the ratio between the magnetic flux density values measured/calculated in the same point without and with the shield (i.e. $\mu_0 H_{appl}/B$).

minimize the amount of space occupied by the shields. The results highlighted that in such an arrangement the magnetic field penetration through the open end cannot be neglected and, as a consequence, at 20 K and for $\mu_0 H_{appl} < 0.4$ T, the addition of the Fe vessel induces a worsening of the shielding efficiency. In contrast, at higher applied fields, where the magnetic flux penetration from the lateral wall becomes significant, the hybrid arrangement shows a SF exceeding by more than a factor of three the SF of the single superconducting cup. Starting from these experimental results we carried out numerical simulations using the vector potential formulation proposed in [22] and found that it is possible, by means of a suitable sizing of the Fe cup, to reduce the gap between the performances of the SC cup and the hybrid system at low applied fields, without compromising the better shielding efficiency of the MgB_2/Fe arrangement at high fields [13].

In this paper we investigate more closely how a suitable sizing of the SC and FM cups can improve the shielding properties of the superimposed SC/FM system. Our goal was to find a superimposed SC/FM cup arrangement with the aspect ratio of height/radius close to unity offering a shielding performance comparable to (or better than) that of the single SC cup at low applied fields. This performance also had to be of the same order of magnitude as that measured for the hybrid system characterized experimentally at high applied fields [6]. To this aim, first the shielding factors of two superimposed cups are calculated as the height of the FM cup changes, keeping the SC cup size constant. Then, using the height differences between the open edge of the SC and FM cups that maximize the shielding efficiency of the hybrid arrangement, we evaluate the shielding efficiency of a multilayer structure made up of two SC and two FM alternating cups. The lateral wall and base thicknesses of the cups are half those used in the bilayer configuration, in order to maintain the mass of the hybrid system nearly unchanged. In both the bilayer and multilayer arrangements the shielding factor analysis is carried out both along the system axis and as a function of the radial position.

The paper is organized as follows. In section 2 we briefly recap the details of the numerical model exploited for the computation of the values of the induction magnetic field, **B**, and the characteristics of the materials used in the simulations. We also list the superimposed cup arrangements investigated in this paper. Section 3 deals with the comparison of the shielding factors evaluated at different applied fields for the configurations reported in Sect. 2. The shielding factor dependences on both the axial and radial coordinates are presented and discussed. The main outcomes are summarized in section 4.

2. Numerical model and sample details

2.1 Numerical model for the computation of the induction field values

The simulations were carried out by a commercial finite-element software [23]. The studied system is made of three/five domains: the superconductor domain(s) (MgB_2), the ferromagnet domain(s) (ARMCO Fe) and the vacuum domain. The external magnetic field is always applied parallel to the cup axis, hereafter called *z*-direction, and its value is fixed through the boundary conditions.

The magnetization process is described starting from Ampere's law. Due to the axisymmetric geometry of our SC/FM arrangements, we worked in cylindrical coordinates. We assumed that the vector potential has only one component, $\mathbf{A}(r,z) = A_\phi(r,z)\mathbf{u}_\phi$. Therefore the magnetic induction is invariant under a rotation around the *z*-axis and has no ϕ-component: $\mathbf{B}(r,z) = \nabla \times \mathbf{A}(r,z) = B_r(r,z)\mathbf{u}_\mathbf{r} + B_z(r,z)\mathbf{u}_z$. Here *r* is the radial coordinate and $\mathbf{u}_r$, $\mathbf{u}_\phi$ and $\mathbf{u}_z$ are the unit vectors along the *r*-, ϕ- and *z*-directions, respectively.

The induction field distribution was calculated for applied fields increasing monotonically. Starting from the virgin state, in agreement with Ref. 22, we imposed a current density flowing in the superconductor and fulfilling the equation:

$$j_\phi(r,z) = j_c \tanh\left(\frac{-A_\phi(r,z)}{A_n}\right)$$

where j_c is the critical current density and A_n is a scaling factor affecting the shape of the current distribution inside the superconductor. We assumed $A_n = 5\cdot10^{-8}$ Wb/m [13]. Since the current density is parallel to the vector potential, it has only the ϕ-component.

The J_c dependence on the local magnetic field is expressed by the relationship [24] $J_c(B) = K\left(\frac{B}{B_{irr}}\right)^\gamma\left(1-\frac{B}{B_{irr}}\right)^\delta$ where γ and δ are parameters depending on the pinning typology [25] and B_{irr} is the irreversibility field. In our case $K = 1.16\cdot10^8$ A/m^2, $\gamma = -0.4$, $\delta = 2.0$ and $B_{irr} = 4.25$ T [13]. Noteworthy, γ and δ values are very close and equal, respectively, to those calculated by Dew-Hugues [25] for the vortex pinning by grain-boundaries, which is the main pinning source expected in a MgB_2 polycrystalline sample [26].

The magnetic flux penetration in the Fe cups was calculated using the *B*-*H* constitutive law of the material [13]. The vacuum domain was drawn as a coaxial cylinder with a radius, R_v, at least 10 times larger than the outer ferromagnetic cup radius. The boundary conditions for the vector potential are $A_\phi(r,z) = \frac{\mu_0 H_{appl} \times R_v}{2}$ on the lateral surface of the cylinder and $A_\phi(r,z) = \frac{\mu_0 H_{appl} \times r}{2}$ on its bases.

This numerical model was proved to reproduce well the values of the induction magnetic field measured experimentally at T = 20 K along the axis of the single MgB_2 cup sketched in Fig. 1(a) and of the hybrid MgB_2/Fe cup arrangement sketched in Fig. 1(b), whose size are reported in the first row of table 1 (configuration no. 1) [13].

2.2 Shield geometry

The schematic pictures of the SC and SC/FM superimposed shields used in the simulations are shown in Fig. 1. Shape and sizes of the SC cup (Fig. 1(a)) correspond to those of the MgB_2 cup characterized experimentally [6, 13]. The sizes of the SC/FM superimposed arrangement tested experimentally [6, 13] are reported in the first row of table 1. All the investigated bilayer shields consists of a SC cup (whose sizes are kept constant and the same as those reported in Fig. 1(a)) inserted into a FM cup. The FM cup size, the height difference between the open edge of the two cups as well as the values of the lateral gap between the cups are listed in table 1.

Since previous calculations [13] have shown that an increase of the lateral gap between the cups leads to a significant SF improvement in the low/intermediate applied field range against a quite negligible worsening at high fields, here we focus on the role played by the presence of a height difference between the open end of the SC and FM cups.

The layout of the multilayer shields is shown in Fig. 1(c). Here, in order to keep the mass of the system nearly unchanged, the lateral wall and base thicknesses of the SC and FM cups are half those used in the bilayer configurations. Some of the dimensions are indicated in the figure, the other ones are listed in the last four rows of table 1 (configurations M1-M4). The value of the lateral gap between the cups was chosen in such a way to maintain the outer diameter of the whole structure the same as that of the bilayer arrangements, while the height differences between the SC and FM cups are those that lead to the best shielding performances in the bilayer configurations.

It is worth remembering that we chose MgB_2 as the SC material for the shield fabrication since, despite its lower working temperature compared to high temperature SC cuprates, it can be used in the polycrystalline state without the current flow being compromised by the grain boundary presence and orientation [27]. Moreover, MgB_2 can be manufactured with techniques such as the liquid Mg infiltration technique in boron preforms [28] that allows obtaining samples of different shapes and easily scalable size [29].

3. Simulation results

3.1 Shielding factor values along the shield axis

First, we calculated the induction field values along the axis of the SC cup and of the SC/FM cup configurations no. 1-8, listed in table 1. Data show evidence of shielding effects also close and outside to the cup edge, as can be seen in Fig. 2 where the curves calculated for the single SC cup are plotted. In order to make easier the comparison of the shielding potential of the SC cup and of the SC/FM superimposed systems, Fig. 3 shows directly the ratios between the SF calculated for each hybrid system and that one calculated for the SC cup alone, SF_{hybrid}/SF_{SC} - corresponding to the induction field ratio B_{SC}/B_{hybrid} - at low (Fig. 3(a)), intermediate (Fig. 3(b)) and high (Fig. 3(c)) applied fields. On the basis of the unsatisfactory results reported in Ref. 7 for arrangements with the FM tube placed inside the SC one, we disregarded configurations with the FM cup placed inside the SC one. Moreover, for sake of comparison, despite the lower value of the lateral gap between the cups, results achieved for the configuration no.1 are also plotted, since this arrangement corresponds to that characterized experimentally [6].

The analysis highlights that the introduction of a height difference between the cup edges is fundamental to improve the shielding efficiency of the superimposed system in the low/intermediate magnetic field range. Indeed, in these systems with a small aspect ratio the magnetic flux penetration from the cup opening is predominant at low applied fields and this edge mismatch reduces the stronger accumulation of the flux lines at the cup opening induced by the addition of the FM vessel. At low applied fields ($\mu_0 H_{appl}$ = 0.04 T) the arrangements with the SC cup protruding above the FM one are the most promising configurations while in the intermediate applied field range ($\mu_0 H_{appl}$ = 0.2 T) also the structures with the FM cup protruding above the SC one start becoming competitive. However, in both cases the ratio SF_{hybrid}/SF_{SC} is always lower than one, evidence that the whole SC solution is still the best.

In contrast, at high applied fields, where the penetration from the lateral/bottom walls becomes significant, the superimposed SC/FM systems always show a better shielding efficiency. The best SF is produced by the arrangements with the highest FM cups, thus reducing more strongly the magnetic pressure at the superconductor lateral walls.

Starting from these results, we investigated the shielding efficiency of multilayer superimposed arrangements consisting of two SC and two FM alternating cups. In order to keep nearly unchanged the mass of the whole system, as well as its inner and outer lateral dimensions, the lateral wall and base thicknesses of the cups are half those used in the bilayer configurations and the lateral gap between the cup was chosen of 0.67 mm. The height difference between the cup edge was assumed of 2 and 3 mm, i.e. the values that provide the most promising results in the bilayer configuration. Also in this case the shielding factor of the superimposed structures is normalized to that of the single

superconducting cup drawn in Fig. 1(a). The main results are summarized in Fig. 4. For the sake of comparison, also the SF ratios for the better and the worse bilayer arrangements are reported.

The new multilayer configurations not only fully recover the gap between the SC and the hybrid solution but also show higher shielding efficiency at low applied fields ($\mu_0 H_{appl}$ = 0.04 T – Fig. 4(a)) if the SC cups protrude above the FM ones. As already happens in the bilayer configuration, in the intermediate field range ($\mu_0 H_{appl}$ = 0.2 T – Fig. 4(b)) the arrangement where the open end of the FM cups is 3 cm higher than that of the SC cups (configuration M4) becomes the most competitive hybrid system, here overcoming the performance of the single SC cup. As expected, at high applied fields all the superimposed arrangements, and in particular the configurations M3 and M4, guarantee the highest shielding factors. However, also the multilayer M1, consisting of SC cups protruding of 2 mm above the FM ones, shows a shielding factor up to three times greater than that of the single SC cup. This, joined to the positive behaviour at low applied fields and to the lower density of MgB_2 compared to Fe, could make this solution preferred if weight constraints were present.

3.2 Shielding factor values as a function of the distance from the shield axis

Since the devices to be shielded generally have a non-negligible lateral extension, we also analysed how the shielding factors change as a function of the distance from the axis of the shield. Fig. 5 shows the induction field values calculated along the radial direction inside the SC cup at a distance of 5.5 mm and 3.5 mm from its edge. At low/intermediate applied fields, *B* decreases as the distance from the cup axis increases. This outcome agrees with a predominant entering of the magnetic flux from the cup opening. On the contrary, at high applied fields, *B* reaches higher values close to the lateral wall. Comparing the SF of the multilayer arrangements to that of the single superconducting cup (Fig. 6), a nearly constant behaviour of the SF ratios occurs in the low/intermediate range of applied fields. Indeed, the shapes of the *B* vs. radial position curves calculated for these hybrid arrangements are similar to those obtained for the SC cup. At high external magnetic fields, even if this trend similarity is confirmed, the slopes of the *B* vs. radial position curves calculated for the hybrid arrangements are generally steeper, thus leading to a decrease of the SF ratios near the lateral wall (Fig. 6(c)). Exceptions are the *B* curves computed inside the arrangements M3 and M4 at a distance of 3.5 mm from the edge of the inner SC cup, which show the same slope as that calculated for the single SC cup.

4. Conclusions

The shielding properties of superimposed SC/FM bilayer and multilayer systems consisting of cylindrical cups, coaxially mounted and with the aspect ratio of height/radius close to unity, were investigated and compared with those of a single SC cup. The shielding factors of all the arrangements were calculated as a function of both the axial and the radial position using an approach based on the vector potential formulation.

Both bilayer and multilayer hybrid arrangements always prove to be the most efficient shielding solution at high external fields, due to the reduction of the magnetic flux density on the external walls of the SC cup induced by the addition of the FM vessel. The best shielding performances are achieved by multilayer structures with the FM cups protruding above the SC ones.

In contrast, at low/intermediate magnetic fields the gain in using the SC/FM solutions is almost negligible. The single SC cup remains the most effective shield if compared to all the examined bilayer configurations and it only performs slightly less well than the multilayer systems. Moreover, in this range of applied fields, the reduction of the effect of the flux line accumulation induced by the FM vessel(s) at the cup opening is found to be the key factor to achieve a competitive hybrid arrangement. This can be obtained by imposing a height difference between the SC and FM cup and/or by enlarging the gap(s) between the lateral walls of the vessels.

These results represent a preliminary guideline for the design of shielding structures intended to use in practical situations where it is necessary to minimize the amount of space occupied by the shield. Possible weight constraints can also affect the choice of the shield structure. To this end, further investigations are in progress aimed at reducing the mass of the FM vessel.

Acknowledgments

We wish to thank F. Gömöry for fruitful discussions. This work was partially supported by the Italian National Institute of Nuclear Physics (INFN) under SR2S-RD experiment.

References

[1] Kamiya K., Warner B.A., DiPirro M.J.: Magnetic shielding for sensitive detectors. Cryogenics **41**, 401-405 (2001)

[2] Denis S., Dusolier L., Dirickx M., Vanderbemden Ph., Cloots R., Ausloos M., Vanderheyden B: Magnetic shielding properties of high-temperature superconducting tubes subjected to axial fields. Supercond. Sci. Technol. **20**, 192-201 (2007)

[3] Rabbers J.J., Oomen M.P., Bassani E., Ripamonti G., Giunchi G.: Magnetic shielding capability of MgB_2 cylinders. Supercond. Sci. Technol. **23**, 125003 (2010)

[4] Omura A., Oka M., Mori K., Itoh M.: Magnetic shielding effects of the superposition of a ferromagnetic cylinder over an HTS cylinder: magnetic shielding dependence on the air gap between the BPSCCO and soft-iron cylinders. Physica C **386**, 506–511 (2003)

[5] Cybart S. A., Wu S. M., Anton S. M., Siddiqi I., Clarke J., Dynes R. C.: Series array of incommensurate superconducting quantum interference devices from $YBa_2Cu_3O_{7-\delta}$ ion damage Josephson junctions. Appl. Phys. Lett. **93**, 182502 (2008)

[6] Gozzelino L., Agostino A., Gerbaldo R., Ghigo G., Laviano F.: Magnetic shielding efficiency of superconducting/ferromagnetic systems. Supercond. Sci. Technol. **25**, 115013 (2012)

[7] Lousberg G.P., Fagnard J.-F., Ausloos M., Vanderbemden P., Vanderheyden B.: Numerical study of the shielding properties of macroscopic hybrid ferromagnetic/superconductor hollow cylinders. IEEE Trans. Appl. Supercond. **20**, 33-41 (2010)

[8] Gömöry F., Solovyov M., Šouc J., Navau C., Prat-Camps J., Sanchez A.: Experimental realization of a magnetic cloak. Science **335**, 1466–1468 (2012)

[9] Gömöry F., Solovyov M. and Šouc J.: Magnetization loop modelling for superconducting /ferromagnetic tube of an ac magnetic cloak. Supercond. Sci. Technol. **28**, 044001 (2015)

[10] Prat-Camps J., Navau C., Sanchez A.: A magnetic wormhole. Scientific Report **5**, 12488 (2015)

[11] Chiampi M., Gozzelino L., Manzin A., Zilberti L.: Thin-shell formulation applied to superconducting shields for magnetic field mitigation. IEEE Trans. Magn. **47**, 4266–4269 (2011)

[12] Gozzelino L., Gerbaldo R., Ghigo G., Laviano F., Agostino A., Bonometti E., Chiampi M., Manzin A., Zilberti L.: DC shielding properties of coaxial MgB2/Fe cups. IEEE Trans. Appl. Supercond. **23**, 8201305 (2013)

[13] Gozzelino L., Gerbaldo R., Ghigo G., Laviano F., Truccato M., Agostino A.: Superconducting and hybrid systems for magnetic field shielding. Supercond. Sci. Technol. **29**, 034004 (2016)

[14] Sirois F., Grilli F.: Potential and limits of numerical modelling for supporting the development of HTS devices. Supercond. Sci. Technol. **28**, 043002 (2015)

[15] Campbell A.M.: An introduction to numerical methods in superconductors. J. Supercond. Nov. Magn. **24**, 27–33 (2011)

[16] Del-Valle N., Navau C., Sanchez A., Chen D.-X.: Tunability of the critical-current density in superconductor-ferromagnet hybrids. Appl. Phys. Lett. **98**, 202506 (2011)

[17] Philippe M.P., Ainslie M.D., Wéra L., Fagnard J.-F., Dennis A.R., Shi Y.-H., Cardwell D.A., Vanderheyden B., Vanderbemden P.: Influence of soft ferromagnetic sections on the magnetic flux density profile of a large grain, bulk Y–Ba–Cu–O superconductor. Supercond. Sci. Technol. **28**, 095008 (2015)

[18] Ainslie M.D., Rodriguez-Zermeno V.M., Hong Z., Yuan W., Flack T.J., Coombs T.A.: An improved FEM model for computing transport AC loss in coils made of RABiTS YBCO coated conductors for electric machines. Supercond. Sci. Technol. **24**, 045005 (2011)

[19] Amemiya N., Miyamoto K., Murasawa S., Mukai H., Ohmatsu K.: Finite element analysis of AC loss in non-twisted Bi-2223 tape carrying AC transport current and/or exposed to DC or AC external magnetic field. Physica C **310**, 30–35 (1998)

[20] Campbell A.M.: A direct method for obtaining the critical state in two and three dimensions. Supercond. Sci. Technol. **22**, 034005 (2009)

[21] Campbell A.M.: A new method of determining the critical state in superconductors. Supercond. Sci. Technol. **20**, 292-295 (2007)

[22] Gömöry F., Vojenčiak M., Pardo E., Šouc J.: Magnetic flux penetration and AC loss in a composite superconducting wire with ferromagnetic parts. Supercond. Sci. Technol. **22**, 034017 (2009)

[23] COMSOL 4.3b (http://comsol.com/)

[24] Kitahara K., Akune T., Matsumoto Y., Sakamoto N.: Scaling law and irreversibility fields in MgB2 superconductors. Physica C **445-448**, 471–473 (2006)

[25] Dew-Hughes D.: Flux pinning mechanisms in type II superconductors. Phil. Mag. **30**, 293–305 (1974)

[26] Martínez E., Mikheenko P., Martínez-López M., Millán A., Bevan A., Abell J.S.: Flux pinning force in bulk MgB_2 with variable grain size. Phys. Rev. B **75**, 134515 (2007)

[27] Gozzelino L., Laviano F., Botta D., Chiodoni A., Gerbaldo R., Ghigo G., Mezzetti E., Giunchi G., Ceresara S., Ripamonti G.: Critical state analysis in bulk MgB_2 by means of a quantitative magneto-optical technique. Philos. Mag. B **82**, 1 (2002)

[28] Giunchi G., Ceresara S., Ripamonti G., Chiarelli S., Spadoni M.: MgB_2 reactive sintering from the elements. IEEE Trans. Appl. Supercond. **13**, 3060–3063 (2003)

[29] Giunchi G., Ripamonti G., Cavallin T., Bassani E.: The reactive liquid Mg infiltration process to produce large superconducting bulk MgB_2 manufacts. Cryogenics **46**, 237–242 (2006)

Table and Figure Captions

Table 1 Geometrical parameters of the SC/FM cup arrangements shown in Figs. 1(b) and (c). All the sizes are in mm. Negative values of d_2 mean that the SC cup(cups) protrudes(protrude) above the FM one(ones). The configuration no. 1 has the same dimensions of the hybrid arrangement characterized experimentally [6, 13].

Fig. 1 Schematic view of the SC cup (a), of the bilayer SC/FM arrangements (b) and of the multilayer SC/FM arrangements (c) used in the calculations. All the sizes are in mm. The values of R_i, R_e, h, d_1, d_2 are reported in table 1. The induction fields were calculated along the dashed lines (axial direction) and the dotted lines (radial direction).

Fig. 2 Induction fields calculated along the SC cup axis (dashed line in Fig. 1(a)) assuming external applied fields $\mu_0 H_{appl}$ = 0.04, 0.2 and 1.0 T. The zero position corresponds to the cup edge, while the hatched frame indicates the internal region of the cup.

Fig. 3 Comparison of the ratios SF_{hybrid}/SF_{SC} calculated for the cup arrangements no. 1-8 as a function of the position along the cup axis (dashed line in Figs. 1(a) and (b)) at $\mu_0 H_{appl}$ = 0.04 T (a), 0.2 T (b), 1.0 T (c). The numbers reported on the curves refer to the arrangement number (see table 1). The zero position corresponds to the SC cup edge, while the hatched frame indicates the internal region of the SC cup.

Fig. 4 Comparison of the ratios SF_{hybrid}/SF_{SC} calculated for the multilayer arrangements M1-M4 as a function of the position along the cup axis (dashed line in Figs. 1(a) and (c)) at $\mu_0 H_{appl}$ = 0.04 T (a), 0.2 T (b), 1.0 T (c). For sake of comparison the better/worse results obtained with the bilayer arrangements (Fig. 3) are also plotted. The labels/numbers reported on the curves refer to the arrangement number (see table 1). The zero position corresponds to the inner SC cup edge, while the hatched frame indicates the internal region of the inner SC cup.

Fig. 5 Induction field computed inside the SC cup, along the radial direction (dotted lines in Fig. 1(a)) at 5.5 mm (lines) and 3.5 mm (symbols) below its edge. Calculations were carried out assuming the external applied fields $\mu_0 H_{appl}$ = 0.04, 0.2 and 1.0 T. The zero position corresponds to the cup axis.

Fig. 6 Comparison of the ratios SF_{hybrid}/SF_{SC} calculated for the multilayer arrangements M1-M4 inside the cup system, as a function of the radial position (dotted lines in Figs. 1(a) and (c)) at 5.5 mm (lines) and 3.5 mm (symbols) below the edge of the inner SC cup. The simulations were carried out assuming external applied fields $\mu_0 H_{appl}$ = 0.04 T (a), 0.2 T (b) and 1.0 T (c). The zero position corresponds to the shield axis.

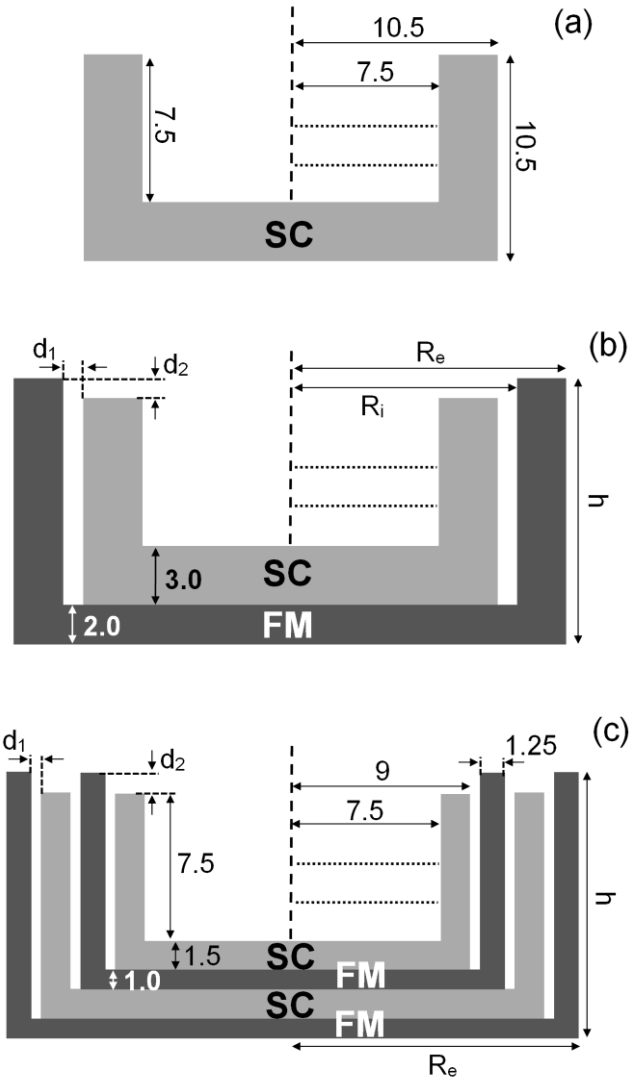
(a)
10.5
7.5
7.5
10.5
SC
(b)
d1
d2
Re
Ri
h
3.0
SC
2.0
FM
(c)
d1
d2
1.25
9
7.5
7.5
h
1.5
SC
1.0
FM
SC
FM
Re

Figure 1

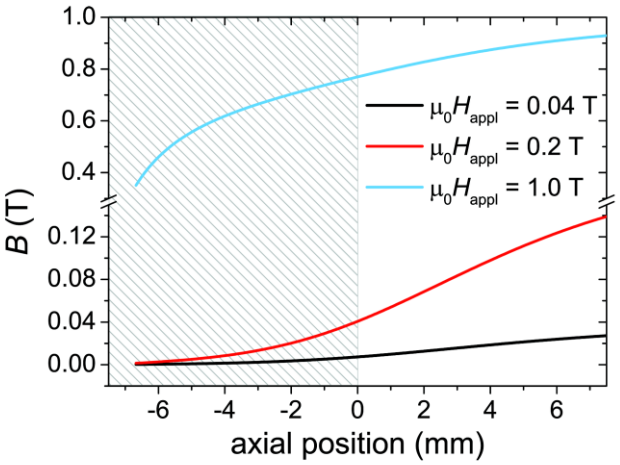
1.0
0.8
0.6
0.4
0.12
0.08
0.04
0.00
B (T)
-6
-4
-2
0
2
4
6
axial position (mm)
μ0Happl = 0.04 T
μ0Happl = 0.2 T
μ0Happl = 1.0 T

Figure 2

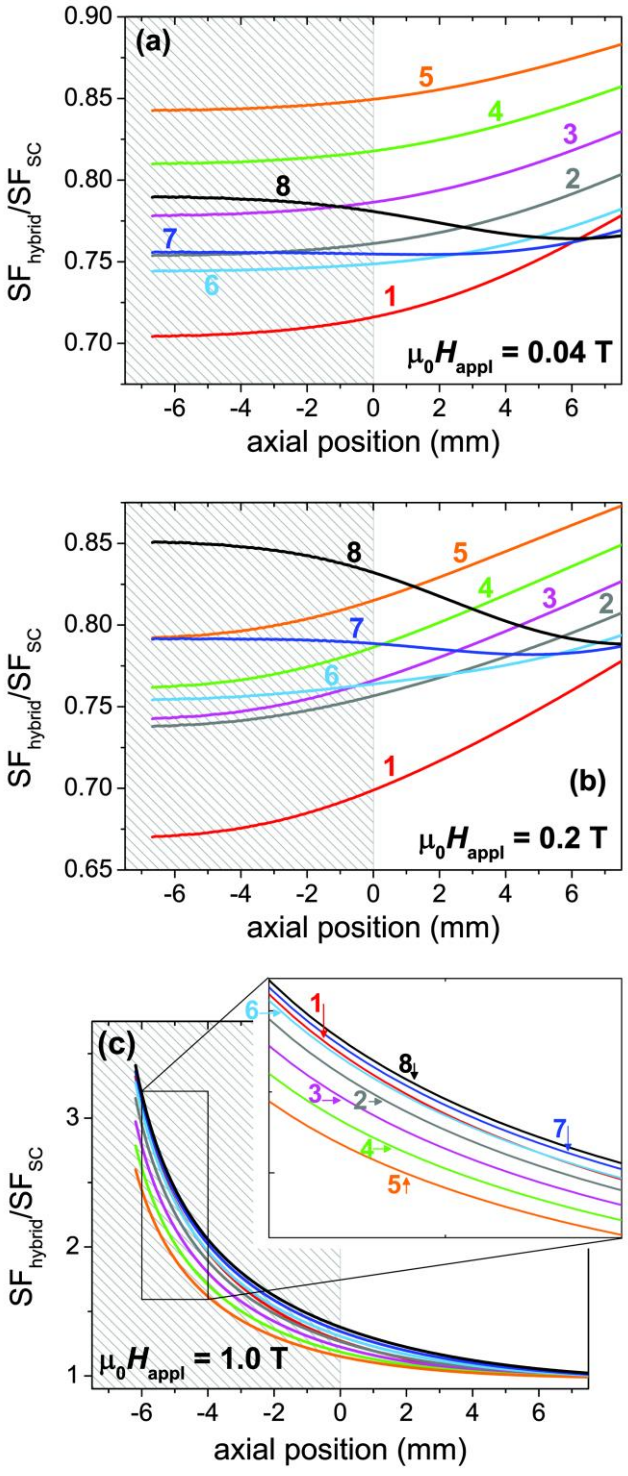
(a)
5
4
3
2
8
7
6
1
$\mu_0 H_{appl}$ = 0.04 T
SF_{hybrid}/SF_{SC}
axial position (mm)
(b)
$\mu_0 H_{appl}$ = 0.2 T
(c)
$\mu_0 H_{appl}$ = 1.0 T

Figure 3

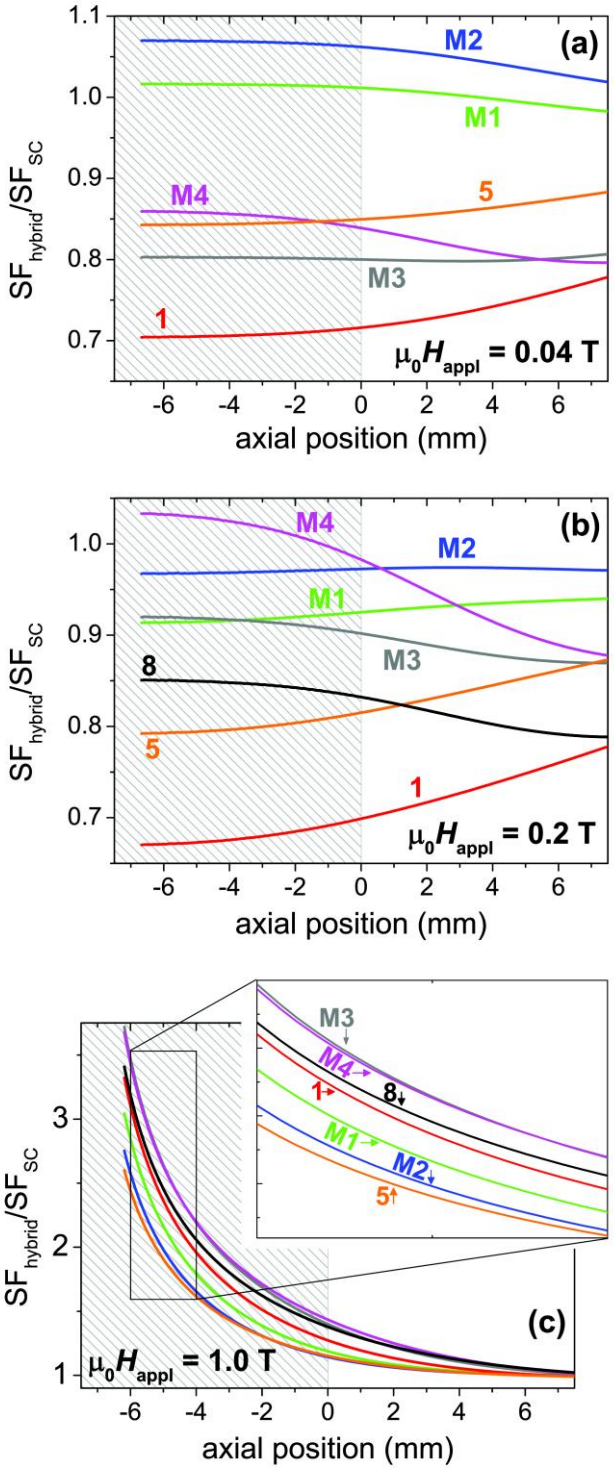
(a)
M2
M1
M4
5
M3
1
$\mu_0 H_{appl}$ = 0.04 T
SF_{hybrid}/SF_{SC}
axial position (mm)
(b)
M4
M2
M1
M3
8
5
1
$\mu_0 H_{appl}$ = 0.2 T
SF_{hybrid}/SF_{SC}
axial position (mm)
M3
M4
1
8
M1
M2
5
(c)
$\mu_0 H_{appl}$ = 1.0 T
SF_{hybrid}/SF_{SC}
axial position (mm)

Figure 4

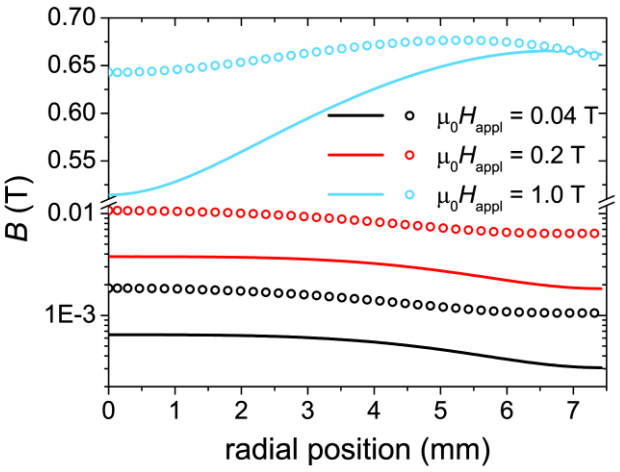
0.70
0.65
0.60
0.55
0.01
1E-3
B (T)
μ0Happl = 0.04 T
μ0Happl = 0.2 T
μ0Happl = 1.0 T
0
1
2
3
4
5
6
7
radial position (mm)

Figure 5

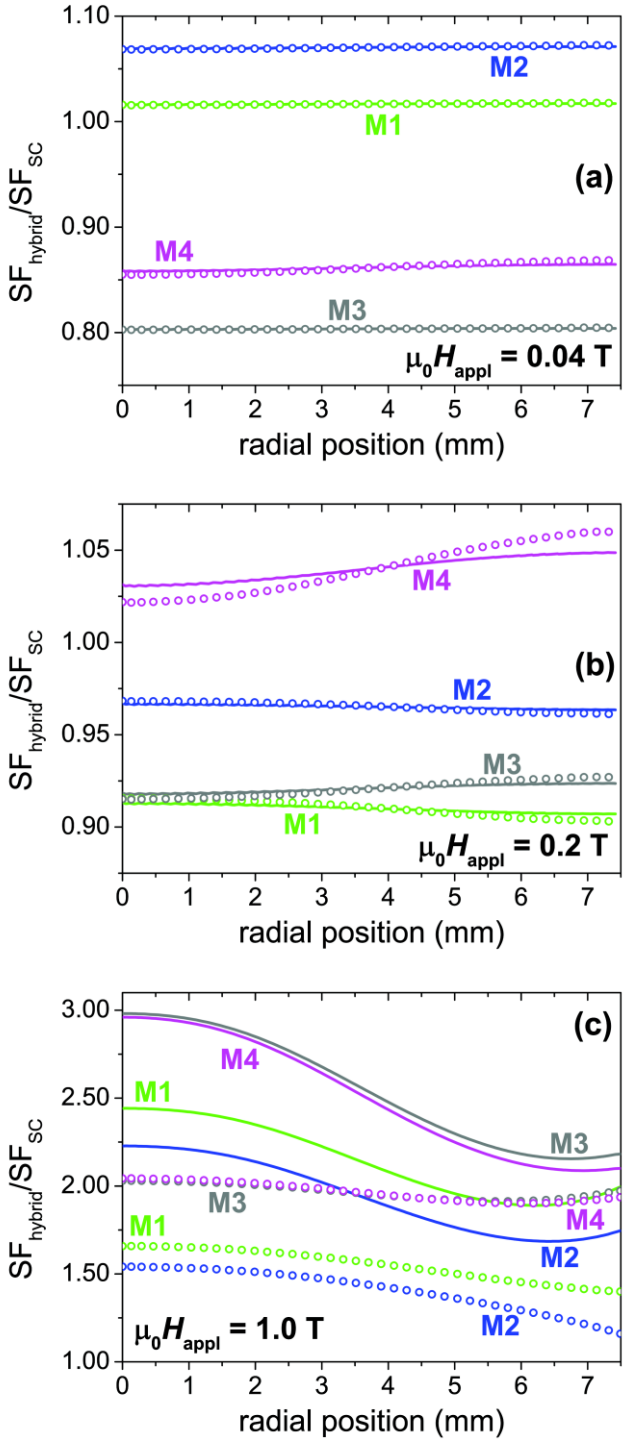
1.10
1.00
0.90
0.80
SF_hybrid/SF_SC
M2
M1
(a)
M4
M3
μ0Happl = 0.04 T
0 1 2 3 4 5 6 7
radial position (mm)
1.05
1.00
0.95
0.90
SF_hybrid/SF_SC
M4
(b)
M2
M3
M1
μ0Happl = 0.2 T
0 1 2 3 4 5 6 7
radial position (mm)
3.00
2.50
2.00
1.50
1.00
SF_hybrid/SF_SC
(c)
M4
M1
M3
M3
M1
M4
M2
M2
μ0Happl = 1.0 T
0 1 2 3 4 5 6 7
radial position (mm)

Figure 6